



Synthesis of Silica Nanoparticles from Silica Sand via Vibration Assisted Alkaline Solution Method

M. S. Hamzah^{a,b}, M. W. Wildan^{*a}, K. Kusmono^a, E. Suharyadi^c

^a Department of Mechanical and Industrial Engineering, Faculty of Engineering, Universitas Gadjah Mada, Yogyakarta, Indonesia

^b Departement of Mechanical Engineering, Tadulako University, Palu, Indonesia

^c Departement of Physics, Faculty of Mathematics and Natural Sciences, Universitas Gadjah Mada, Yogyakarta, Indonesia

PAPER INFO

Paper history:

Received 31 January 2022

Received in revised form 15 March 2022

Accepted 02 April 2022

Keywords:

Morphology

Dielectric Properties

Alkaline Fusion

Speaker Membrane

ABSTRACT

The effect of frequency of speaker membrane vibration on the grain size of the silica nanoparticles (SNP) was investigated. SNP was synthesized using the alkaline fusion method under the vibration of the membrane speaker. Variations of membrane vibration used in this research were 0, 50, 100, and 200 Hz. The material compositions, crystal structure, and morphology of the synthesized SNP were characterized using X-ray fluorescence (XRF), X-ray diffraction (XRD), and transmission electron microscopy (TEM), respectively. Meanwhile, its dielectric property was determined using impedance spectroscopy. The results showed that the SNP consisted of 99.35% silica and corresponded to the crystalline structure of quartz silica. The SNP size was decreased with increasing vibration frequencies. The smallest size of SNP (9.04 ± 1.9 nm) was obtained at a frequency of 200 Hz. Moreover, the dielectric constant and dielectric losses were increased with an increase in membrane vibration frequency due to the decrease of SNP size.

doi: 10.5829/ije.2022.35.07a.09

1. INTRODUCTION

Indonesia is a country that is rich in potential natural minerals, including oxide materials such as silica sand [1, 2]. There are many silica grains of sand in Indonesia, spread all over the country regions, such as in Poso Regency, Central Sulawesi. Silica sand obtained from Poso has a high SiO₂ content that can be utilized in industrial materials [3]. It can be processed into silica nano particles (SNP) through a top-down or bottom-up method [4]. For the last-mentioned method, SNP was obtained through chemical reactions using precursors. Particles in nanometer size provide advantages such as good electrical, optical, and magnetic properties [5]. SNP is widely used in industry because of its high productivity and low production costs [6]. Previous researchers have reported various methods in synthesizing the SNP, including hydrothermal [7, 8], sol-gel [9], sodium silicate solution [10, 11], alkaline fusion [12-14], and precipitation method [15]. These methods are generally

carried out with stirring to inhibit grain growth; however, the resulting particles have still lacked. Other researchers have also developed several methods to obtain smaller sizes of particles. Indira and Malathi [16] reported the synthesis of hydroxyapatite nanoparticles for biomedical applications using ultrasonic and microwave methods. Rusianto et al. [17] reported the synthesizing of magnetite nanoparticles assisted by mechanical vibration. Yu et al. [18] reported the method of utilizing ultrasonic/mechanical vibrations in metallurgical processes such as welding and metal casting to control metal particle size. It was also reported that ultrasonic vibrations in the welding process can smooth particles and improve the mechanical properties of welds [18-20].

SNP can exist in three crystal structures, namely quartz, tridymite, and cristobalite. It has a large surface area, good heat resistance, high mechanical strength, and can be used as catalyst precursors, adsorbents, and composite filters, easy modification, good chemical stability, and low cytotoxicity [5, 21, 22]. SNP can be

*Corresponding Author Institutional Email: m_wildan@ugm.ac.id
(M. W. Wildan)

used to improve the cooling effect and efficiency of the vapor compression refrigeration cycle [23]. Nowadays, SNP is commonly used in various industries such as rubber, filler, catalyst carriers, [24-27], food, automobile, energy storage materials, piezoelectric materials, paints, medical, electronics, and others [28, 29]. A dielectric material is an insulator with high resistivity that can be polarized if there is an electrostatic dipole or under an external electric field [30]. Previous researchers have reported the impact of the nano-silica amount on its dielectric properties [31, 32]. The combination methods between alkaline fusion and membrane vibration can be used in synthesizing silica nanoparticles by heating the sample at a specific temperature, depositing it and then it followed by vibrating and stirring until the pH is neutral. This method is advantageous because it does not require a long time and does not require high energy [13]. As a result, the synthesis process takes place effectively and efficiently to produce nanoparticles. The SNP synthesis method that has been used so far has limitations, including the lack of nanoparticles produced, and the particle size is not controlled, so a new approach is needed.

This study reports the new method of SNP synthesizing by combining the alkaline fusion with membrane speaker vibration, which offers mass production of SNP with controllable size. This study aimed to investigate the effect of the frequency of speaker membrane vibration on the particle size and the dielectric properties.

2. MATERIALS AND METHODS

The raw material used to synthesize silica nanoparticles was obtained from silica sand on Poso Island, Central Sulawesi, Indonesia [33]. Sodium hydroxide and hydrochloric acid used in this work were bought from Merck (Germany).

Silica nanoparticles (SNP) was prepared by using a combination of alkaline fusion and speaker membrane methods as follows. Briefly, the raw silica sand was cleaned and dried in an oven. The metallic elements within the silica sand were removed using several permanent magnets to obtain non-metallic compounds with high concentrations. Silica sand was crushed using a ball mill to find smaller particle sizes. Then, the crushed silica sand was sieved into < 200 mesh using a sieve shaker. Silica sand concentrates were mixed with pro-analyst NaOH in a ratio of 1: 1 by weight fraction, then heated at 600°C for 1 h. The heated mixture of silica sand and NaOH was put into a beaker glass which was filled with distilled water. The beaker glass was placed on a hot plate magnetic stirrer and heated at about 75°C with a stirring speed of 500 rpm. Stirring was combined with the vibration of the speaker membrane with different

frequencies of 0, 50, 100, and 200 Hz with a duration of 30 min, respectively. The solution was stirred for 16 h while the pre-analytical HCl solution was titrated with a concentration of 37% at 2 M. The solution would form a residue (silica gel) at the pH of 7-8. The silica precipitates were filtered using Whatman glass microfiber filter (grade 42, 2.5 µm) and then washed with distilled water until it turned white. The washed silica residues were dried in an oven at 100°C for 15 h and then characterized. Variations of membrane vibration used were 0, 50, 100, and 200 Hz, respectively, then referred to as SNP0, SNP50, SNP100, and SNP200. The schematic of the synthesis of SNP with the alkaline fusion method combined with a speaker membrane can be seen in Figure 1.

The chemical composition and microstructure of SNP were characterized using X-ray fluorescence (XRF) (RIGAKU-NEX-QC+QuanTES) and transmission electron microscope (TEM) (JEOL JEM-1400), respectively. Images of each SNP from the TEM image were analysed using Image J software to determine the grain size distribution. X-ray Diffraction analysis (Bruker D2 Phaser) was used to identify the crystalline phase of each SNP. Then, the synthesized SNPs at various frequencies of 0, 50, 100, and 200 Hz were compacted in a 15 mm diameter cylindrical die with pressure of 75 MPa to produce green bodies. The green bodies were sintered at 1360°C for 2 h with a heating rate of 10°C/min. The dielectric properties of the sintered samples were tested using a computerized impedance spectroscopy device with a sine frequency generator that produced a modulating frequency in the range of 10 to 500 kHz.

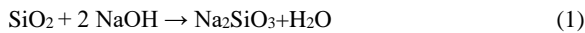
3. RESULT AND DISCUSSION

3. 1. Synthesis of Silica Nanoparticles The main mineral in silica sand is quartz which has a tetrahedron



Figure 1. Schematic illustration of the synthesis method of SNP

structure, where at high temperatures, each tetrahedron will be separated from each other because the bonds between the anions and cations are not very strong [34], so that NaOH binds silica to form sodium metasilicate that was separated from other minerals. Consecutively, sodium metasilicate was titrated with HCl to produce hydrous silica and silicic acid. Then, the white residue in a gel was washed with distilled water to remove the remaining solution. The chemical reactions of this synthesis process are presented in Equations (1) and (2) [35].



3. 2. Composition

Table 1 shows the chemical composition of the silica sand and SNP as revealed by XRF. It was found that both silica sand and SNP have the main component of SiO₂ around 99.35-99.64%. From Table 1, it can be also observed that the content of the same components is indicated by both silica sand and SNP. It can be concluded that the synthesis of SNP did not change the composition of silica sand.

3. 3. Crystal Structures

The XRD diffractogram of the raw material (silica sand) and the obtained SNP are presented in Figure 2. As observed, 2θ of the peaks of raw material and SNP are not significantly different. As compared to JCPDS (33-1161 card number) for silica quartz, the appeared sharp peaks show that the raw material and SNP are in the quartz phase with the related 2θ are 20.90°, 26.70°, 36.58°, 39.51°, 42.49°, 45.83°, 50.18°, 54.91°, 60.64°, 68.16°. In line with the literature, quartz is one of the crystalline phases of silicon oxide that formed at temperatures below 870°C [36]. From Figure 2, it can be seen that various vibration frequencies of the speaker membranes (0, 50, 100, and 200 Hz) did not affect the SNP crystal structure. The SNP synthesized with various frequencies exhibits a quartz phase. Furthermore, X-ray diffraction is not only used to identify the crystal structure but also is used to determine the crystal size by using the Scherer equation as shown in Equation (3) [17]:

TABLE 1. Chemical composition of silica sand and the SNP

Composition	Silica sand (wt%)	SNP (wt%)
SiO ₂	99.64	99.35
TiO ₂	0.20	0.18
Fe ₂ O ₃	0.06	0.06
NiO	0.03	0.02
CuO	0.01	0.01
ZnO	0.01	0.01
Others	0.05	0.35

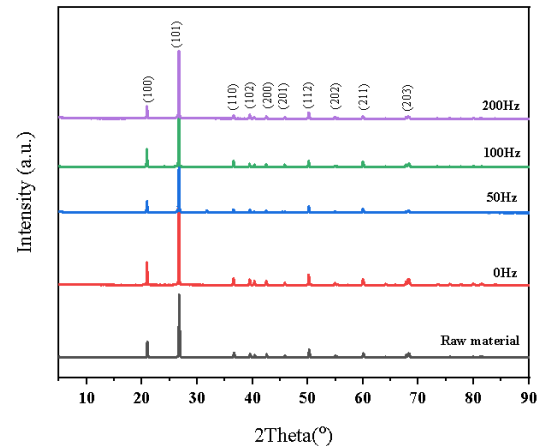


Figure 2. XRD diffractogram of synthesized SNP with various frequencies of speaker membrane vibration

$$D = (0.9 \lambda) / (\beta \cos \theta) \quad (3)$$

where D is the size of the crystallite diameter (nm), λ is the wave length of the x-ray used, θ is the angle (1/2 peak angle), and β is the full width of half maximum (FWHM). The four peak at 2θ of 20.90°, 26.70°, 36.58°, and 50.18° are used as the basis for determining the size of the crystal diameter. It was found that the SNP crystal size obtained at different frequencies (0, 50, 100, and 200 Hz) are 10.8, 5.0, 1.04, and 0.9 nm, respectively. Based on the XRD results, it can be concluded that the synthesis of SNP by the alkaline fusion method combined with a speaker membrane did not change the crystal structure of silica sand. This finding is in consistent with XRF results as previously discussed. In addition, increasing the vibration frequency reduces the crystal size of the SNP. This is associated with an increase in frequency can increase the nucleation rate and then result in smaller crystal size [37].

3. 4. Morphology Studies

Figure 3 shows the TEM images and the size distribution of SNP for various speaker membrane vibration frequencies. The size of silica particles is in the nanometer order, which depends on the frequency of the speaker membrane vibration. From Figure 3, it was found that the particle sizes of SNP at different frequencies of 0, 50, 100, and 200 Hz are 14±3.34, 12±2.54, 11±2.56, and 9±1.95 nm, respectively. The SNP size decreases with the imposition of speaker membrane vibrations. This indicates that the higher vibration frequency leads to a smaller size of produced SNP. Thus, the SNP size decreases with the application of speaker membrane vibrations. This is because the vibrational frequency of the membrane can inhibit crystal growth. After all, the arrangement of atoms becomes disturbed or unstable when speaker membrane vibration is applied. In comparison, the increase in frequency will increase the vibration energy, where the vibration energy

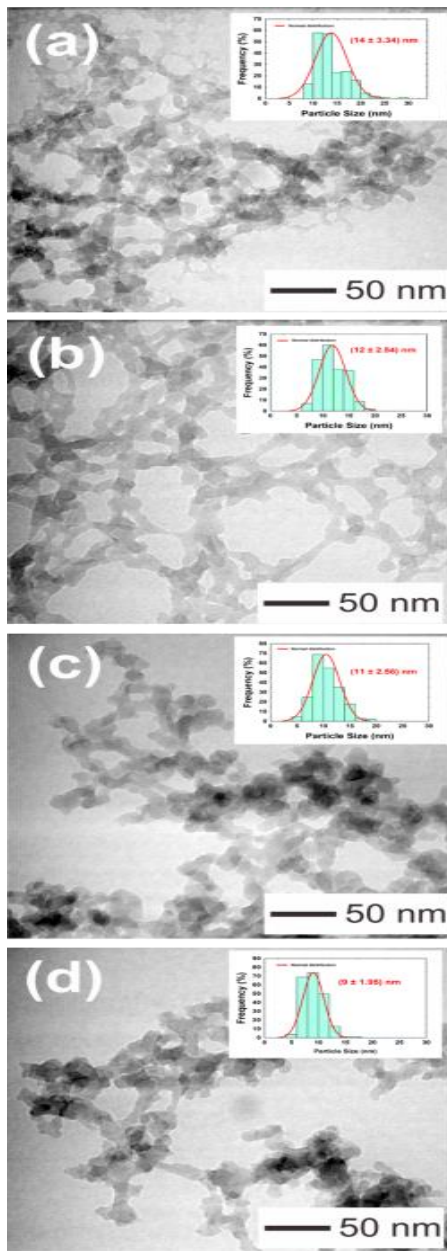


Figure 3. TEM images of SNP and its particle distributions with various speaker membrane vibration frequencies: a). 0 Hz, b). 50 Hz, c). 100 Hz, and d). 200 Hz

can inhibit the growth of crystals to form smaller particles [17]. The TEM results are consistent with the XRD results as mentioned before, where increasing the vibration frequency decreased the SNP crystal size.

3. 5. Dielectric Properties

Figure 4 shows the frequency dependence of real dielectric permittivity (ϵ') and dielectric loss (ϵ''). The dielectric permittivity and dielectric loss of SNP0, SNP50, SNP100, and SNP200 are decreased with the increase of frequency. Meanwhile, the decrease in real dielectric permittivity and dielectric

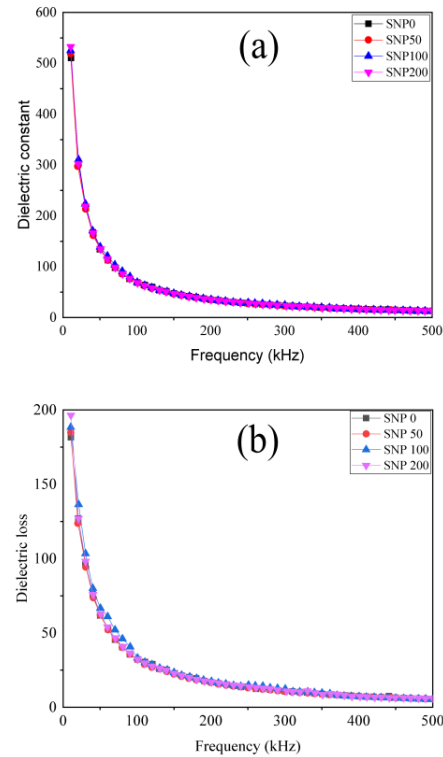


Figure 4. Frequency-dependent plot of permittivity for SNP0, SNP50, SNP100, and SNP200, (a) dielectric constant, and (b) dielectric loss

loss is significant in the range of 10 kHz to 200 kHz and be saturated over 200 kHz. The real dielectric constant and the imaginary dielectric constant are calculated by Equations (4), (5) and (6).

$$\Phi = \arctan(V_c/V_r) \tag{4}$$

$$\epsilon' = (d \sin \theta) / (2\pi f \epsilon_0 A |Z|) \tag{5}$$

$$\epsilon'' = \epsilon' \tan \delta \tag{6}$$

where ϕ is the capacitance impedance which determined by $|Z| = V_c \max / V_r \max \times R$, ϵ' is proportional to the energy stored and ϵ'' is proportional to the energy lost or dissipated. While the loss tangent value is the ratio between the permittivity of the imaginary dielectric to the permittivity of the real dielectric. The two parts of the permittivity (real dielectric and dielectric loss) in the low-frequency region have strong dispersion. The real dielectric constant and dielectric loss show low values at high frequencies and increase with decreasing frequency. This phenomenon is comparable to that reported in the literature [37, 38].

The sample exhibits strong dielectric dispersion behavior at low frequencies due to the significant contribution of space charge polarization to dielectric properties, and the dielectric constant remains nearly

constant at higher frequencies [39, 40]. Another thing that causes is the inability of electrons to align their position with a given electric field so that the polarization between grain decreases which affects the dielectric value.

The decrease in grain size causes an increase in the number of grains and grain boundaries, which directly reduces the number of dipole moments. The poling plane does not have many domains to exchange, so the poling process is inefficient in a particle. Similar types of results have been reported for oxide ceramics [41]. Furthermore, four types of polarization, i.e., dipolar, ionic, electronic, and interfacial polarization, contribute to the total polarization of the dielectric material [42]. The different magnitude of the real dielectric value in each sample is due to differences in grain size. Decreasing the grain size leads to a higher dielectric value [39, 43]. Moreover, the highest dielectric occurs in SNP200, which is in agreement with the TEM results. Other factors that affect the dielectric value are defects, residual stress at the interface, porosity, grain boundaries, and variations in crystal structure parameters [44].

4. CONCLUSIONS

Silica nanoparticles sourced from natural sand were successfully synthesized using the alkaline fusion method assisted by speaker membrane vibration. XRF analysis showed SiO₂ content of 99.36% by weight and a similar to the silica content of silica sand. XRD analysis indicated that the identified phase of SNP was quartz. TEM observations showed that the silica nanoparticle's size was decreased with an increase in speaker membrane vibration frequency. The dielectric constant and dielectric loss show high values at low frequencies and decrease at high frequencies, and this occurs in all samples. With an increasing frequency of the speaker membrane vibration during synthesis, the value of the dielectric constant was found to be higher, and this was the effect of decreasing the grain size of silica nanoparticles.

5. ACKNOWLEDGEMENTS

This work was supported by the Ministry of Education, Culture, Research and Technology of the Republic of Indonesia and Indonesia Endowment Fund for Education (LPDP) with contract number of KET-574/LPDP.4/2020.

6. REFERENCES

1. Hidayat, T. and Fitrianingrum, L., "Ecology and sociology analysis for mineral resources management in indonesia", in IOP

Conference Series: Earth and Environmental Science, IOP Publishing. Vol. 483, No. 1, (2020), 012030.

2. Ismail, A., Saputri, L., Dwiatmoko, A., Susanto, B. and Nasikin, M., "A facile approach to synthesis of silica nanoparticles from silica sand and their application as superhydrophobic material", *Journal of Asian Ceramic Societies*, Vol. 9, No. 2, (2021), 665-672, <https://doi.org/10.1080/21870764.2021.1911057>
3. Darwis, D., Khaerani, R. and Iqbal, I., "Pemurnian dan karakterisasi silika menggunakan metode purifikasi (leaching) dengan variasi waktu milling pada pasir kuarsa desa pasir putih kecamatan pamona selatan kabupaten poso", *Natural Science: Journal of Science and Technology*, Vol. 6, No. 2, (2017), <https://doi.org/10.22487/25411969.2017.v6.i3.9201>
4. Biswas, A., Bayer, I.S., Biris, A.S., Wang, T., Dervishi, E. and Faupel, F., "Advances in top-down and bottom-up surface nanofabrication: Techniques, applications & future prospects", *Advances in Colloid and Interface Science*, Vol. 170, No. 1-2, (2012), 2-27, <https://doi.org/10.1016/j.cis.2011.11.001>
5. Khan, I., Saeed, K. and Khan, I., "Nanoparticles: Properties, applications and toxicities", *Arabian Journal of Chemistry*, Vol. 12, No. 7, (2019), 908-931, <https://doi.org/10.1016/j.arabj.2017.05.011>
6. Yu, K., Liang, Y., Ma, G., Yang, L. and Wang, T.-J., "Coupling of synthesis and modification to produce hydrophobic or functionalized nano-silica particles", *Colloids and Surfaces A: Physicochemical and Engineering Aspects*, Vol. 574, No., (2019), 122-130.
7. Potapov, V., Efimenko, Y., Fediuk, R. and Gorev, D., "Effect of hydrothermal nanosilica on the performances of cement concrete", *Construction and Building Materials*, Vol. 269, (2021), 121307, <https://doi.org/10.1016/j.conbuildmat.2020.121307>
8. Zainuri, M., "Synthesis of sio nanopowders containing quartz and cristobalite phases from silica sands", *Materials Science-Poland*, Vol. 33, No. 1, (2015), 47-55, doi. <https://doi.org/10.1515/msp-2015-0008>
9. Owoeye, S.S., Abegunde, S.M. and Oji, B., "Effects of process variable on synthesis and characterization of amorphous silica nanoparticles using sodium silicate solutions as precursor by sol-gel method", *Nano-Structures & Nano-Objects*, Vol. 25, No., (2021), 100625, doi. <https://doi.org/10.1016/j.nanoso.2020.100625>
10. El-Didamony, H., El-Fadaly, E., Amer, A.A. and Abazeed, I.H., "Synthesis and characterization of low cost nanosilica from sodium silicate solution and their applications in ceramic engobes", *Boletín de la Sociedad Española de Cerámica y Vidrio*, Vol. 59, No. 1, (2020), 31-43, doi. <https://doi.org/10.1016/j.bsecv.2019.06.004>
11. Owoeye, S.S., Jegede, F.I. and Borisade, S.G., "Preparation and characterization of nano-sized silica xerogel particles using sodium silicate solution extracted from waste container glasses", *Materials Chemistry and Physics*, Vol. 248, (2020), 122915, <https://doi.org/10.1016/j.matchemphys.2020.122915>
12. Wahyudi, A., Amalia, D. and Sariman, S., "Preparation of nano silica from silica sand through alkali fusion process", *Indonesian Mining Journal*, Vol. 16, No. 3, (2013), 149-153.
13. Ayele, L., Pérez-Pariente, J., Chebude, Y. and Díaz, I., "Conventional versus alkali fusion synthesis of zeolite a from low grade kaolin", *Applied Clay Science*, Vol. 132, (2016), 485-490, <https://doi.org/10.1016/j.clay.2016.07.019>
14. Shi, B. and Chang, Q., "Green synthesis of fly ash-based zeolite y by mixed alkali fusion method", *Micro & Nano Letters*, Vol. 16, No. 11, (2021), 540-545, <https://doi.org/10.1049/ma.2021.12083>
15. Jyoti, A., Singh, R.K., Kumar, N., Aman, A.K. and Kar, M., "Synthesis and properties of amorphous nanosilica from rice husk and its composites", *Materials Science and Engineering: Conference Series: Earth and Environmental Science*, IOP Publishing. Vol. 483, No. 1, (2020), 012030.

- B, Vol. 263, (2021), 114871, <https://doi.org/10.1016/j.mseb.2020.114871>
16. Indira, J. and Malathi, K., "Comparison of template mediated ultrasonic and microwave irradiation method on the synthesis of hydroxyapatite nanoparticles for biomedical applications", *Materials Today: Proceedings*, Vol. 51, (2022), 1765-1769, <https://doi.org/10.1016/j.matpr.2021.03.028>
 17. Rusianto, T., Wildan, M.W. and Abraha, K., "Various sizes of the synthesized Fe₃O₄ nanoparticles assisted by mechanical vibrations", (2015).
 18. Yu, M., Zhao, H., Xu, F., Chen, T., Zhou, L., Song, X. and Ma, N., "Influence of ultrasonic vibrations on the microstructure and mechanical properties of al/ti friction stir lap welds", *Journal of Materials Processing Technology*, Vol. 282, (2020), 116676, <https://doi.org/10.1016/j.jmatprotec.2020.116676>
 19. Lei, Z., Bi, J., Li, P., Li, Q., Chen, Y. and Zhang, D., "Melt flow and grain refining in ultrasonic vibration assisted laser welding process of az31b magnesium alloy", *Optics & Laser Technology*, Vol. 108, (2018), 409-417, <https://doi.org/10.1016/j.optlastec.2018.07.015>
 20. Zhou, S., Wang, B., Wu, D., Ma, G., Yang, G. and Wei, W., "Follow-up ultrasonic vibration assisted laser welding dissimilar metals for nuclear reactor pump can end sealing", *Nuclear Materials and Energy*, Vol. 27, (2021), 100975, <https://doi.org/10.1016/j.nme.2021.100975>
 21. Tolba, G.M., Bastaweesy, A., Ashour, E., Abdelmoez, W., Khalil, K.A. and Barakat, N.A., "Effective and highly recyclable ceramic membrane based on amorphous nanosilica for dye removal from the aqueous solutions", *Arabian Journal of Chemistry*, Vol. 9, No. 2, (2016), 287-296, <https://doi.org/10.1016/j.arabjc.2015.05.009>
 22. Ma, M., Li, H., Xiong, Y. and Dong, F., "Rational design, synthesis, and application of silica/graphene-based nanocomposite: A review", *Materials & Design*, Vol. 198, (2021), 109367, <https://doi.org/10.1016/j.matdes.2020.109367>
 23. Rahman, M.W.U., Rahman, M., Sarker, M., Rashid, F. and Al Mahmud, M.M., "Synthesis of nano silica particle from silica sand and characterization of nano silica based r134a refrigerant", *Materials Today: Proceedings*, Vol. 46, (2021), 6816-6821, <https://doi.org/10.1016/j.matpr.2021.04.368>
 24. Sattayanurak, S., Noordermeer, J.W., Sahakaro, K., Kaewsakul, W., Dierkes, W. and Blume, A., "Silica-reinforced natural rubber: Synergistic effects by addition of small amounts of secondary fillers to silica-reinforced natural rubber tire tread compounds", *Advances in Materials Science and Engineering*, Vol. 2019, (2019), <https://doi.org/10.1155/2019/5891051>
 25. Lee, S.Y., Kim, J.S., Lim, S.H., Jang, S.H., Kim, D.H., Park, N.-H., Jung, J.W. and Choi, J., "The investigation of the silica-reinforced rubber polymers with the methoxy type silane coupling agents", *Polymers*, Vol. 12, No. 12, (2020), 3058, <https://doi.org/10.3390/polym12123058>
 26. Torbati-Fard, N., Hosseini, S.M. and Razzaghi-Kashani, M., "Effect of the silica-rubber interface on the mechanical, viscoelastic, and tribological behaviors of filled styrene-butadiene rubber vulcanizates", *Polymer Journal*, Vol. 52, No. 10, (2020), 1223-1234, <https://doi.org/10.1038/s41428-020-0378-x>
 27. Borzouyi Kutenayi, S., Kiahosseini, S. and Talebpour, M., "The effect of caspian sea water on corrosion resistance and compressive strength of reinforced concrete containing different SiO₂ pozzolan", *International Journal of Engineering, Transactions A: Basics* Vol. 30, No. 10, (2017), 1464-1470, doi: 10.5829/ije.2017.30.10a.06
 28. Jittabut, P., "Effect of nanosilica on mechanical and thermal properties of cement composites for thermal energy storage materials", *Energy Procedia*, Vol. 79, (2015), 10-17, <https://doi.org/10.4028/www.scientific.net/amr.1131.182>
 29. Hashemi, S. and MirzaeiMoghadamb, I., "Influence of nanosilica and polypropylene fibers on bond strength of reinforcement and structural lightweight concrete", *Polymer*, Vol. 900, (2014), <https://doi.org/10.5829/idosi.ije.2014.27.02b.10>
 30. Martinez-Vega, J., "Dielectric materials for electrical engineering, John Wiley & Sons, (2013).
 31. Li, Y., Tian, M., Lei, Z., Xu, X. and Wang, S., "Effect of silicon dioxide nano-filler on dielectric and space charge properties of epoxy resin", *High Voltage Engineering*, Vol. 44, (2018), 1870-1877, <https://doi.org/10.13336/j.1003-6520.hve.20180529019>
 32. Mentlik, V. and Michal, O., "Influence of SiO₂ nanoparticles and nanofibrous filler on the dielectric properties of epoxy-based composites", *Materials Letters*, Vol. 223, (2018), 41-44, doi: <https://doi.org/10.1016/j.matlet.2018.04.021>
 33. Ukhtiyani, I., Darwis, D. and Iqbal, I., "Purifikasi dan karakterisasi silika (SiO₂) berbasis pasir kuarsa dari desa pasir putih kecamatan pamona selatan kabupaten poso", *Natural Science: Journal of Science and Technology*, Vol. 6, No. 3, (2017), <https://doi.org/10.22487/25411969.2017.v6.i3.9201>
 34. Schweigert, I., Lehtinen, K., Carrier, M.J. and Zachariah, M.R., "Structure and properties of silica nanoclusters at high temperatures", *Physical Review B*, Vol. 65, No. 23, (2002), 235410, doi: 10.1103/PhysRevB.65.235410.
 35. Asadi, Z. and Norouzbeigi, R., "Synthesis of colloidal nanosilica from waste glass powder as a low cost precursor", *Ceramics International*, Vol. 44, No. 18, (2018), 22692-22697, <https://doi.org/10.1016/j.ceramint.2018.09.050>
 36. Vatalis, K.I., Charalambides, G. and Benetis, N.P., "Market of high purity quartz innovative applications", *Procedia Economics and Finance*, Vol. 24, (2015), 734-742.
 37. Jain, A., Panwar, A.K. and Jha, A., "Influence of milling duration on microstructural, electrical, ferroelectric and piezoelectric properties of ba_{0.9}sr_{0.1}zr_{0.04}ti_{0.96}o₃ ceramic", *Ceramics International*, Vol. 42, No. 16, (2016), 18771-18778.
 38. Kumar, A., Kumarb, A. and Sharmaa, K., "Investigation of dielectric properties of Ni/N-TiO₂/P-Si/Al heterojunction in wide range of temperature and voltage", doi: 10.5829/ije.2022.35.04a.09.
 39. El-Menshawly, O., El-Sissy, A., El-Wazery, M. and Elsad, R., "Electrical and mechanical performance of hybrid and non-hybrid composites", *International Journal of Engineering*, Vol. 32, No. 4, (2019), 580-586, <https://doi.org/10.5829/ije.2019.32.04a.16>
 40. Sari, K., Utomo, A.B.S., Abraha, K., Kartini, E., Yulianti, E. and Suharyadi, E., "Effect of milling time on the microstructure and dielectric properties of chitosan nanopowder", *International Journal of Nanoelectronics & Materials*, Vol. 13, No. 1, (2020), doi: 10.1088/0022-3719/7/17/024
 41. Martirena, H. and Burfoot, J., "Grain-size effects on properties of some ferroelectric ceramics", *Journal of Physics C: Solid State Physics*, Vol. 7, No. 17, (1974), 3182, doi: 10.1088/0022-3719/7/17/024.
 42. Kim, H.N. and Suslick, K.S., "The effects of ultrasound on crystals: Sonocrystallization and sonofragmentation", *Crystals*, Vol. 8, No. 7, (2018), 280, <https://doi.org/10.3390/cryst8070280>
 43. Hu, S., Luo, C., Li, P., Hu, J., Li, G., Jiang, H. and Zhang, W., "Effect of sintered temperature on structural and piezoelectric properties of barium titanate ceramic prepared by nano-scale precursors", *Journal of Materials Science: Materials in Electronics*, Vol. 28, No. 13, (2017), 9322-9327, <https://doi.org/10.1007/s10854-017-6670-7>
 44. Kumar, S., Supriya, S., Pradhan, L.K., Pandey, R. and Kar, M., "Grain size effect on magnetic and dielectric properties of barium hexaferrite (BHF)", *Physica B: Condensed Matter*, Vol. 579, (2020), 411908, <https://doi.org/10.1016/j.physb.2019.411908>

Persian Abstract

چکیده

اثر فرکانس ارتعاش غشای بلندگو بر اندازه دانه نانوذرات سیلیس (SNP) مورد بررسی قرار گرفت. SNP با استفاده از روش همجوشی قلیایی تحت ارتعاش بلندگوی غشایی سنتز شد. تغییرات ارتعاش غشا در این تحقیق ۰، ۵۰، ۱۰۰ و ۲۰۰ هرتز بود. ترکیبات مواد، ساختار کریستالی و مورفولوژی SNP سنتز شده به ترتیب با استفاده از فلورسانس اشعه ایکس (XRF)، پراش پرتو ایکس (XRD) و میکروسکوپ الکترونی عبوری (TEM) مشخص گردید. در همین حال، ویژگی دی الکتریک آن با استفاده از طیفسنجی امپدانس تعیین شد. نتایج نشان داد که SNP از ۹۹/۳۵ درصد سیلیس تشکیل شده و با ساختار کریستالی سیلیس کوارتز مطابقت دارد. اندازه SNP با افزایش فرکانس ارتعاش کاهش یافت. کوچکترین اندازه 9.04 ± 1.9 SNP نانومتر در فرکانس ۲۰۰ هرتز به دست آمد. علاوه بر این، ثابت دی الکتریک و تلفات دی الکتریک با افزایش فرکانس ارتعاش غشا به دلیل کاهش اندازه SNP افزایش یافت.
